J Mater Sci: Mater Electron **(2024) 35:1434**

Synthesis of Bi_2S_3-sensitized TiO_2 photoanodes for enhanced photovoltaic performance in solar cell application

Abhijit T. Supekar[1,2], Pankaj K. Bhujbal[2], Almas M. Mujawar[2], Sandesh R. Jadkar[2], Shoyebmohamad F. Shaikh[3], Sopan M. Rathod[1], Suhas Kowshik[4], and Nithesh Naik[4,*]

[1] *Abasaheb Garware College, Pune, Maharastra 411004, India*
[2] *Advanced Physics Laboratory, Department of Physics, Savitribai Phule Pune University, Pune, Maharastra 411007, India*
[3] *Department of Chemistry, College of Science, King Saud University, P.O. Box 2455, Riyadh 11451, Saudi Arabia*
[4] *Department of Mechanical and Industrial Engineering, Manipal Institute of Technology, Manipal Academy of Higher Education, Manipal, Karnataka 576104, India*

Received: 4 March 2024
Accepted: 9 July 2024
Published online: 18 July 2024

ABSTRACT

The synthesis of Bi_2S_3 nanoparticles for sensitizing TiO_2 photoanodes were synthesized through a cost-effective and straightforward approach using modified chemical bath deposition (M-CBD) or successive ionic atomic layer adsorption reactions (SILAR) at room temperature. Initially, a TiO_2 seed layer was synthesized at room temperature via the chemical bath deposition method, followed by deposition of a mesoporous TiO_2 layer using the doctor blade method. This study investigated the influence of the number of SILAR cycles and the choice of counter electrodes on the performance of Bi_2S_3/TiO_2-based photoelectrodes. Characterization of the prepared Bi_2S_3/TiO_2 photoanode involved various techniques, including X-ray diffraction, UV–Vis spectroscopy, scanning electron microscopy, and Raman spectroscopy, enabling the analysis of its structural, optical, and morphological properties. The Bi_2S_3/TiO_2-based cell exhibits a maximum conversion efficiency of 0.8%, demonstrating the potential of this combination for photovoltaic applications. This study contributes to the field of solar cell technology by presenting a novel approach for sensitizing TiO_2 photoanodes with Bi_2S_3 nanoparticles, offering insights into the optimization of fabrication parameters and performance enhancement strategies for future device design and development.

Address correspondence to E-mail: nithesh.naik@manipal.edu

E-mail Addresses: abhijittsupekar91@gmail.com; pankajbhujbal22@gmail.com; mujawaralmas02@gmail.com; sandesh@physics.unipune.ac.in; shoyeb.chemist@gmail.com; smragc@rediffmail.com; suhas.kowshik@manipal.edu

https://doi.org/10.1007/s10854-024-13181-4

1 Introduction

The utilization of conventional energy resources leads to environmental pollution and energy crises, and overcoming the utilization of renewable and clean energy resources is an alternate. The utilization of solar energy helps reduce the energy crisis. The utilization of solar energy is essential because it is both clean and eco-friendly. Solar cell devices can convert light energy into electrical energy. Semiconductor-sensitized solar cells possess many advantages, such as a high absorption coefficient, constant power output, tunable energy bandgap, and generation of multiple electron–hole pairs with high-energy excitons [1]. Metal-oxide semiconductors are wide bandgap materials with large surface areas for quantum dot absorption. These semiconductors were deposited on transparent conducting oxides, such as indium-doped tin oxide and fluorine-doped tin oxide, with thicknesses of 10–13 μm. Metal oxides such as titanium oxide (TiO_2) [2], zinc oxide (ZnO) [3, 4], indium oxide (In_2O_3) [5, 6], niobium oxide (Nb_2O_5) [7], tungsten oxide (WO_3) [8], and tin oxide (SnO_2) [9, 10] have been widely studied for their fabrication. TiO_2 has been extensively studied owing to its potential optical and electronic properties, which increase the adsorption of quantum dots and enhance photoconversion efficiency. However, the hopping mechanism limits the efficient charge transfer from TiO_2. TiO_2, widely studied metal oxide, is known for its unique optoelectronic properties and wide bandgap (3.2 eV) structure, and is classified into Rutile, Anatase, and Brookite crystal structures. Many narrow bandgap materials such as CdSe, PbS, CdS, Sb_2S_3, and Bi_2S_3 have been used as sensitizers [11–16]. Bi_2S_3 was mainly in the form of bismuthinite. The color of Bi_2S_3 is lead gray to brown, and the melting point and density of Bi_2S_3 are 850 °C and 6.780 gm/cm^3, respectively. Bi_2S_3 is a direct bandgap material that belongs to the V–VI group. The bandgap of Bi_2S_3 is suitable for light harvesting; it is less toxic than PbS- and CdS-based sensitizers, the dispersibility of Bi_2S_3 is good, and either powder or thin films can be synthesized. Various techniques are available for the synthesis of Bi_2S_3 such as electrochemical deposition, [17] chemical bath deposition, [18] and successive ionic layer adsorption and reaction (SILAR) [19–21].

Among these synthetic methods, SILAR/M-CBD is one of the most suitable and common, owing to its facile processing, versatile application to different surfaces and nanostructures, proper coating thickness, and packing density. Bi_2S_3 deposited using the SILAR method is either a thin film or QDs, and the bandgap of Bi_2S_3 is 1.3 − 2.2 eV [22, 23]. It is near the near-infrared region and has a relatively large absorption coefficient; it has applications in solution-processed photodetectors, thermoelectric devices, photosensitizers, solar cells, and supercapacitors. Bi_2S_3 is also an exciting candidate for use in polymer-nanoparticle hybrid solar cells. The objective of this study was to improve the performance of the Bi_2S_3-based solar cells. According to a literature review, the performance of Bi_2S_3-based solar cells does not exceed 2% [19]. To improve the performance of Bi_2S_3-based solar cells, a variety of research strategies have been used, such as surface passivation, co-sensitization, and optimization of the electrolyte and counter electrodes, and details of the strategy and comparative boost in the performance were mentioned in our previously published review article [19]. Here, we focus on an optimized number of SILAR cycles for loading Bi_2S_3 on a mesoporous TiO_2 layer and the impact of the counter electrode on solar cell performance.

The present work demonstrates the synthesis of TiO_2 photoelectrodes for solar cell applications. The Bi_2S_3 nanoparticles were synthesized using the SILAR method. Sandwiched TiO_2/Bi_2S_3 solar cell was measured using a carbon counter electrode and polysulfide electrolyte under a solar simulator assembly. The effect of counter electrodes on the performance of solar cells is significant; therefore, optimization of the counter electrodes is an essential parameter. A good counter electrode has the following properties: 1. high catalytic activity, 2. Good conductivity, and 3. Stability [24, 25]. The solar cell performance was measured using carbon (C) and copper tin sulfide (CTS) counter electrodes. CTS is a promising candidate for replacing Pt counters in DSSC [26]. In this study, we used a SILAR-synthesized CTS/FTO thin film as the counter electrode for a Bi_2S_3/TiO_2-based solar cell. Synthesis of TiO_2 compact film was done by chemical bath deposition [27]. Deposition of mesoporous TiO_2 layers on the seed layer of the TiO_2 film was done using the doctor blade method. For the sensitization of TiO_2 films, Bi_2S_3 was used as a sensitizer. Deposition of Bi_2S_3 on TiO_2 films was done using the SILAR method. A polysulfide electrolyte was used to measure IV performance. Fabrication of CTS counter electrodes was done using the SILAR method [28]. The direct bandgap material like CTS possesses a bandgap within the range of 1.45 eV and the absorption coefficient of CTS is high. CTS can

be synthesized using several methods such as Spray Pyrolysis, chemical bath deposition, SILAR, and sputtering. [29].

In this study, synthesis of the Bi_2S_3/TiO_2 photoelectrodes using cost-effective and simple methods such as chemical bath deposition, doctor blades, and SILAR was performed. SILAR is one of the cheapest methods for the synthesis of metal chalcogenide materials at room temperature. Here, we synthesized Bi_2S_3 nanocrystals for the sensitization of TiO_2 by SILAR method at room temperature. The sensitizer loading on the TiO_2 mesoporous layer was directly proportional to the number of SILAR cycles. Here, we used CTS as the counter electrode for JV characteristic measurements. As per a literature survey, the utilization of CTS as a counter for the JV measurement of Bi_2S_3/TiO_2-based photoelectrodes has not been reported. Here, the Conversion efficiency was higher than that of the carbon counter electrode. The present report also highlights the role of counter electrodes in the performance of Bi_2S_3-coated TiO_2-based solar cells.

Deposition methods such as SILAR and CBD are cost-effective and simple; however, these methods have limitations such as complexity in multilayer deposition, which is time-consuming and requires careful control of the reaction conditions. Choosing the appropriate method depends on cost and compatibility, and methods such as spray pyrolysis, spin coating, thermal evaporation, and hydrothermal methods are useful for material synthesis and film deposition. High-quality crystalline films were obtained using these methods.

2 Experimental details

2.1 Chemicals used

All the chemicals used in this study were without further purification and bought from SRL, Sigma-Aldrich, Thomas Baker, and High Purity Laboratory Chemicals HPLC.

2.2 Preparation of TiO_2/Bi_2S_3 electrode

This study used all the chemicals without further purification and bought from SRL, Sigma-Aldrich, Thomas Baker, and HPLC. The following steps were involved in the formation of the TiO_2/Bi_2S_3 electrode:

2.2.1 *Deposition of TiO_2 compact layer*

In this study, we used a TiO_2 compact film to avoid back contact. The chemical bath deposition method is very cost-effective and does not require sophisticated instruments, and compact TiO_2 is deposited on transparent conducting oxides such as (FTO). The substrates were cleaned via ultrasonication in absolute ethanol, and thoroughly cleaned with acetone. The seed layer is prepared by the chemical bath deposition method using 5 ml $TiCl_3$,1 M NaOH, and 20 ml double-distilled water (DW). The prepared seed layer was annealed at 450 °C [27].

2.2.1.1 Preparation of paste and deposition of mesoporous TiO_2 layer on FTO The preparation of the paste is an important step in the fabrication of metal-oxide layers. Commercial TiO_2 [P25] nanopowder (0.5 g), ethyl cellulose (0.30 g), terpineol (2.72 g), and Acetyl Acetone (0.5 ml) were used to prepare the TiO_2 paste, all of which were of AR grade and were purchased from Loba Chemie. Pvt. Ltd. One of the advantages of using ethanol for the preparation of paste is the volatile nature of ethanol, which easily evaporates when subjected to a small amount of heat treatment in an incubator. The prepared TiO_2 slurry was deposited on a transparent conductive oxide (FTO) substrate using the doctor blade method. The wet TiO_2 films were dried in an incubator for 24 h. Subsequently, the dried mesoporous TiO_2 layer was annealed at 450 °C. for 1 h in a muffle furnace [30].

2.2.2 *Sensitization of TiO_2 photoelectrode by using Bi_2S_3 nanoparticles*

Bi_2S_3 nanoparticles sensitized TiO_2 Films using the SILAR method; 0.003 M Bismuth Nitrate (Bi $(NO_3)_2$) and 0.015 M Sodium Sulfide Na_2S were the sources of cationic and anionic precursors, respectively, in double-distilled water. The sensitized films were then annealed. The steps involved in the deposition of Bi_2S_3 are shown in Fig. 1. Here, mesoporous TiO_2 film is dipped in beaker 1 for 20 s after that, the film is rinsed in beaker 2. The third beaker contained an anion source film dipped for 20 s, and the same film was rinsed for 10 s in beaker 4, completing the one SILAR cycle. The same procedure was done 5-25

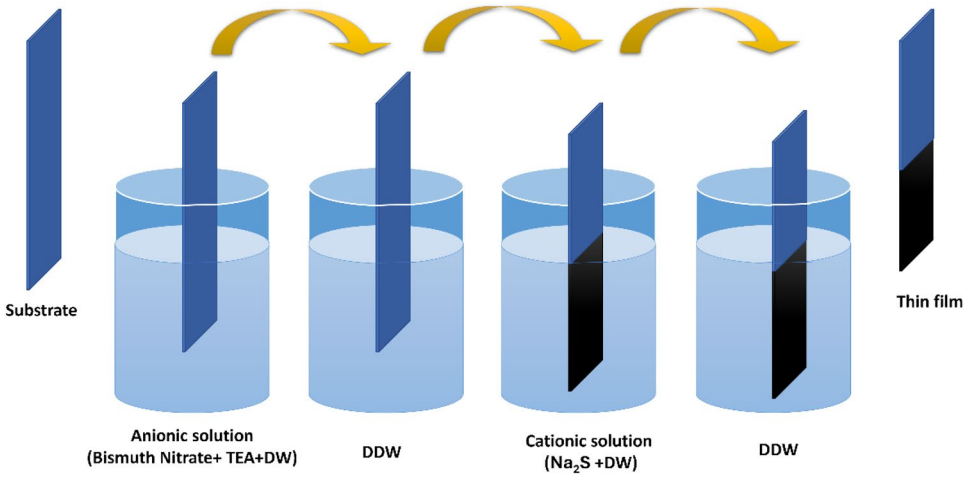

Fig. 1 Steps involved in the sensitization of TiO_2 films using Bi_2S_3 nanoparticles by SILAR method

times with very fine and uniform deposition of Bi_2S_3 occurring on the TiO_2 film [31, 32].

2.3 Preparation of polysulphide electrolyte

Polysulfide electrolytes are preferred for semiconductor-sensitized solar cells. Polysulfides were prepared using Na_2S and sulfur powder in ethanol, methanol, and water.

2.4 Synthesis of CTS counter electrode on FTO

The counter electrode directly influences R_{series}, and thus, the Fill Factor, which is why optimization and choosing an appropriate counter electrode is the most important part of the fabrication of solar cells [33]. A CTS counter electrode was synthesized using the SILAR method [28].

2.5 Device fabrication

The Bi_2S_3/TiO_2 photoanode and CTS counter electrode were combined to form a sandwich solar cell spacer separating the two electrodes. Polysulfide electrolytes are used as redox mediators in photoanodes and counter electrodes. The performance of the Bi_2S_3/TiO_2-based solar cells was measured using a solar simulator assembly. A schematic representation of the Bi_2S_3/TiO_2-based solar cells is shown in Fig. 2a.

Figure 2b shows a Schematic Representation of the band alignment of the Bi_2S_3/TiO_2 electrode: the conduction band potential of Bi_2S_3 (0.7) is more negative

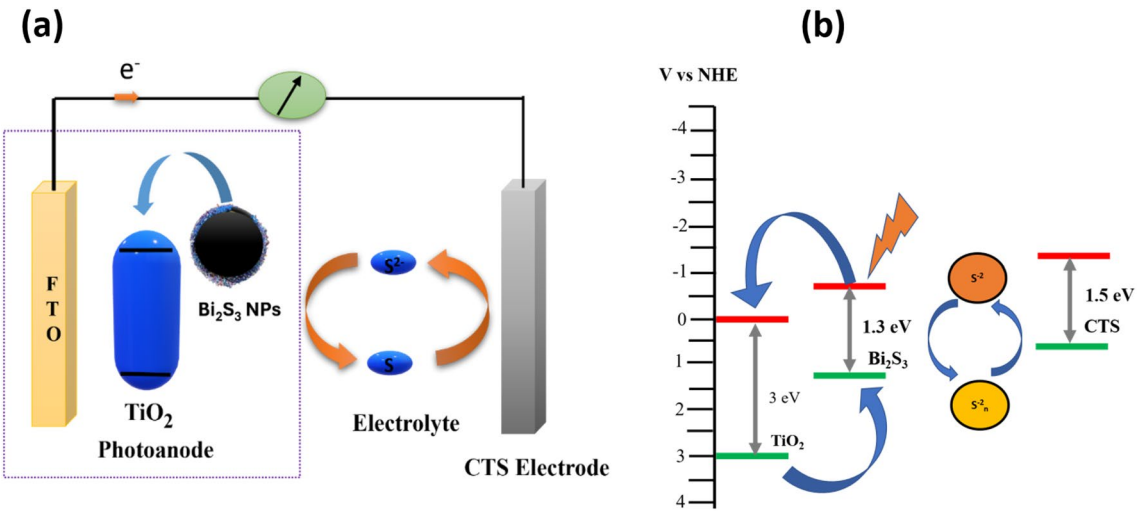

Fig. 2 Schematic representation (**a**) Bi_2S_3/TiO_2 solar cell (**b**) band alignment of Bi_2S_3/TiO_2 solar cell [34]

than that of TiO_2, and the valence band (VB) is more cathodic than the VBs of TiO_2; therefore, photoexcited electrons from the conduction band of Bi_2S_3 jump towards TiO_2, which is useful for enhancing the photovoltaic performance of Bi_2S_3/TiO_2-based solar cell [34].

3 Result and discussion

3.1 Structural properties analysis (X-ray diffraction techniques)

Figure 3 shows the XRD patterns of FTO, TiO_2, and Bi_2S_3-sensitized TiO_2 film using an X-ray diffractometer Bruker D8 with CuKα radiation (1.54 Å) in the range of 20°–80°. Peaks attributed to # are the peaks of FTO, XRD analysis of TiO_2 film revealed that peaks corresponding to 25.5, 27.6, 37.8, 48.2, 53.9, 62.5 degrees are the peaks of TiO_2 (Peaks of TiO_2 were denoted by *) having tetragonal anatase and rutile structure. Peaks are matched with JCPDS 21–1272. Average crystallite size was estimated to be 27 nm, calculated by Scherrer formula, Fig. 3 also shows XRD graphs of Bi_2S_3/TiO_2 photoelectrode peaks of Bi_2S_3 denoted by (B), and the observed characteristics peak at 22.4, 23.7, 28.7, 31.9, 33.05, 34.02, 35.7, 39.2, 40.23, 42.8, 45.6, 46.6, 51.06, and 52.78° are assigned to the (220), (101), (230), (221), (301), (330), (240), (041), (340), (421), (002),(431), (441), and (132) planes of orthorhombic Bi_2S_3 (JCPDS No. 75–1306), it shows Bi_2S_3 is successfully deposited on TiO_2. The average crystallite size was estimated to be 25 nm.

3.2 Optical properties study

JASCO UV–Vis Spectrometers were used to measure the optical properties of Bi_2S_3/TiO_2 films on FTO, and the UV–Vis spectra were measured in the range of 200–1000 nm. The absorption spectra of the TiO_2 films are shown in Fig. 4. Spectral analysis revealed that the Bi_2S_3-sensitized TiO_2 photoanode had an absorption band that extended from the ultraviolet to the visible region, indicating that the sensitization of TiO_2 with Bi_2S_3 nanoparticles improved its light absorption capabilities across a wider range of wavelengths. This is in contrast to the unsensitized TiO_2 film, which primarily absorbs light in the ultraviolet region, thus limiting its efficiency in harnessing light energy for potential applications. When Bi_2S_3 nanoparticles were loaded onto the TiO_2 photoanode, the absorption width extended towards the visible wavelength region, enabling the sensitized TiO_2 photoanode to capture a broader range of light wavelengths, potentially improving its efficiency and performance in solar cell applications. [35]

The shift in the absorption peak from 421 to 630 nm as the number of deposition cycles increased from 5 to 25 in the Bi_2S_3/TiO_2 films indicates a significant change in the absorbed energy and optical properties of the material. To calculate the shift in the absorbed energy, we can use the following formula:

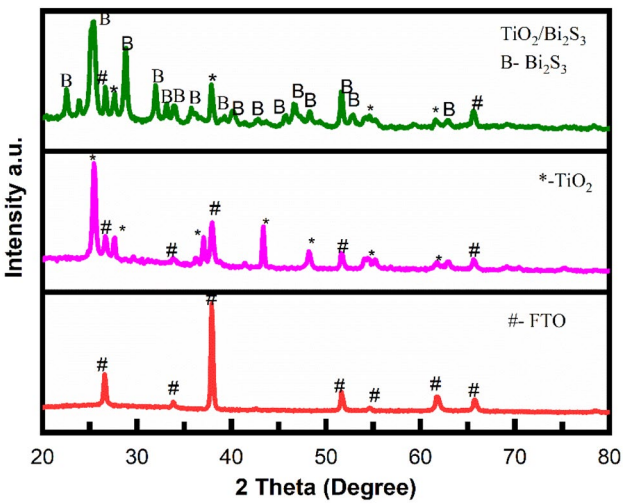

Fig. 3 XRD of bare FTO, TiO_2 film deposited by doctor blade method and Bi_2S_3-sensitized TiO_2 film

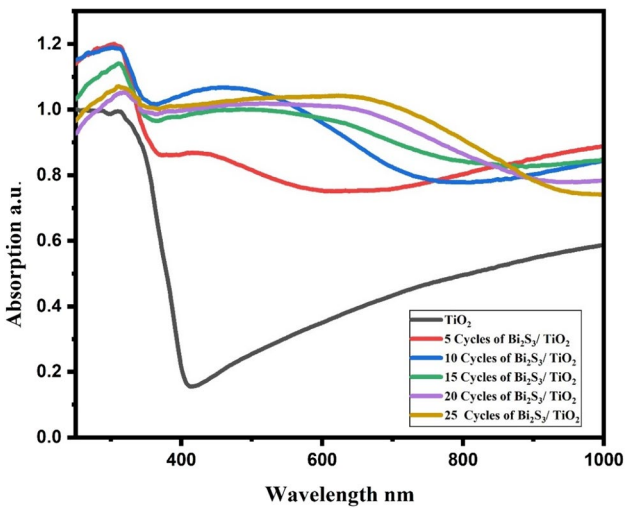

Fig. 4 UV–Visible spectra of Bi_2S_3/TiO_2 films

$$\Delta E = \frac{hc}{\lambda_2} - \frac{hc}{\lambda_1}. \quad (1)$$

The equation relates the shift in the absorbed energy (ΔE), Planck's constant (h), speed of light (c), initial wavelength (421 nm), and final wavelength (630 nm). The shift in the absorbed energy was 0.98 eV.

3.3 Morphological analysis by scanning electron microscopy (SEM)

The surface morphologies of the TiO_2 compact and doctor-bladed films were recorded using a JEOL JSM-6360A Scanning Electron microscope [SEM]. Figures 5a (A to F) show SEM micrographs of the TiO_2 film deposited by the simple Doctor Blade method on a chemical bath-deposited compact TiO_2 layer showing granular morphology. Bi_2S_3 nanoparticles were successfully loaded onto the TiO_2 film, and figures

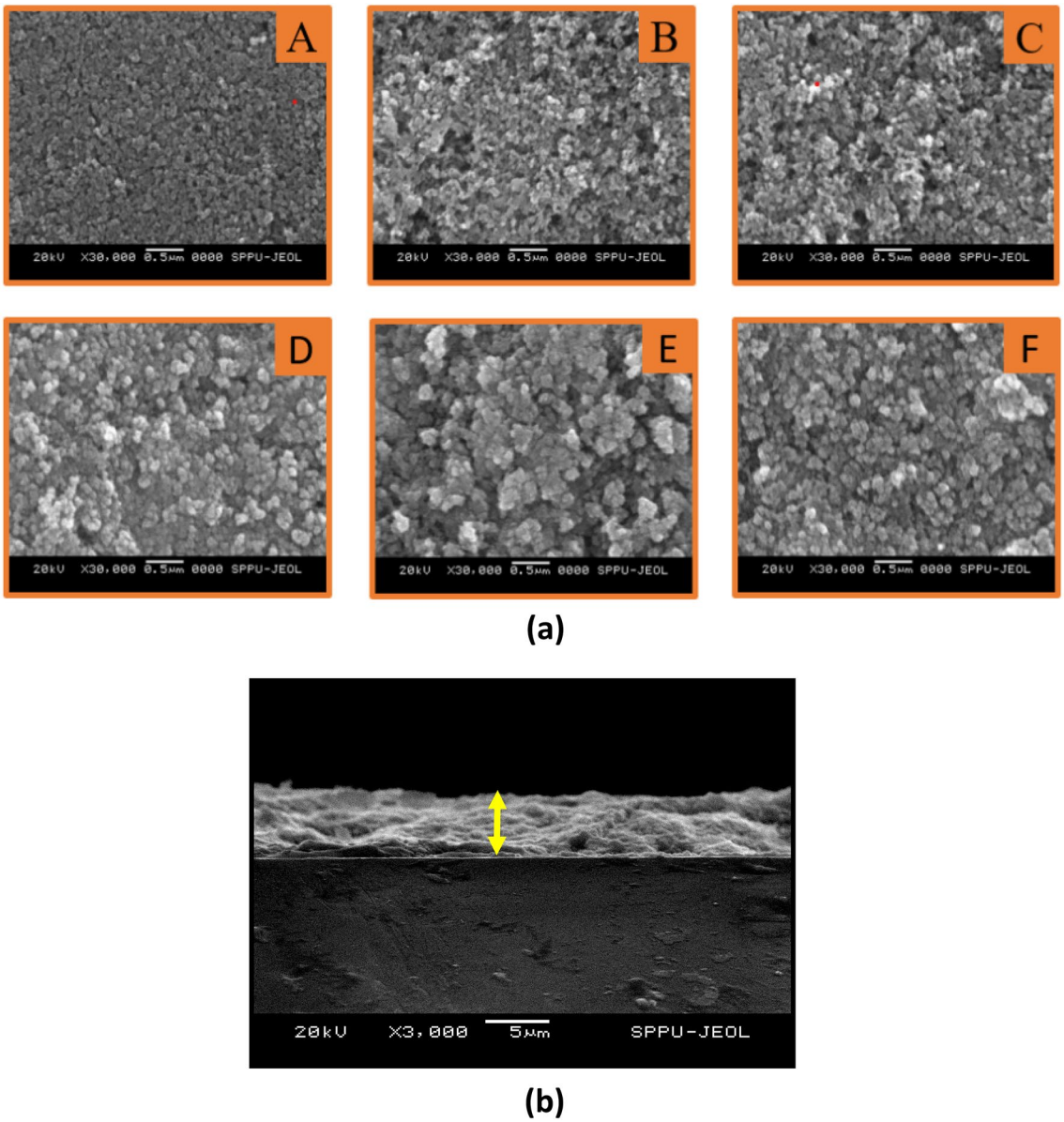

Fig. 5 **a** SEM micrographs of **A** TiO_2, **B** Bi_2S_3/TiO_2, – 5 SILAR cycles, **C** Bi_2S_3/TiO_2, – 10 SILAR cycles, **D** Bi_2S_3/TiO_2, – 15 SILAR cycles, **E** Bi_2S_3/TiO_2, – 20 SILAR cycles, **F** Bi_2S_3/TiO_2, – 25 SILAR cycles. **b** SEM cross section of TiO_2 film

Table 1 Atomic percentage of Ti. O, Bi, and S

Material composition	No. of SILAR cycles	Ti At %	O At%	Bi At %	S At %
TiO_2	–	18.80	81.20	–	–
Bi_2S_3/TiO_2	5	17.30	81.66	0.77	0.27
Bi_2S_3/TiO_2	10	15.90	81.48	1.55	1.07
Bi_2S_3/TiO_2	15	16.37	77.72	3.23	2.67
Bi_2S_3/TiO_2	20	16.61	73.34	4.84	5.21
Bi_2S_3/TiO_2	25	15.36	76.36	4.32	3.97

B–F show that Bi_2S_3 deposited TiO_2 films by various SILAR cycles (5–25). It indicates that as the number of SILAR cycles increased, the size of Bi_2S_3 increased. Figure 5b shows the SEM cross section of the TiO_2 film; the thickness of the doctor-bladed TiO_2 film is approximately 5–7 µm. The deposition of Bi_2S_3 was confirmed by energy-dispersive spectroscopy (EDS) analysis, as shown in Figure S1 (Supporting Information). The atomic percentages of Bi and S increased as the number of SILAR cycles increased, as shown in Figure S1a–f. The variation in the atomic percentages of Bi and S (the number of SILAR cycles varied from (5–25)) is shown in Table 1.

This study demonstrates that we successfully deposit Bi_2S_3 nanoparticles on TiO_2 using the SILAR method. The number of SILAR cycles was varied from 5 to 25, and the atomic percentage of Bi_2S_3 increased with the number of cycles. The EDS results confirmed the deposition of Bi_2S_3, showing increasing atomic percentages of Bi and S with more cycles. The atomic percentages of Ti and O decreased as the Bi_2S_3 content increased, indicating the uniform coating of Bi_2S_3 on TiO_2. SEM and EDS results showed that the SILAR technique could tune the Bi_2S_3 loading on TiO_2 by adjusting the number of cycles. In summary, the characterization techniques confirmed the controlled coating of TiO_2 with Bi_2S_3 nanoparticles using the SILAR method by varying the number of deposition cycles.

3.4 Raman spectroscopy

Raman spectroscopy was used to determine the phases and crystallinity of the prepared samples. The Raman spectra of the TiO_2 and Bi_2S_3/ TiO_2 samples are shown in Figs. 6a and b, respectively. Raman Spectra of TiO_2/Bi_2S_3 samples were collected in the range of 100–1000 cm^{-1}. Figure 6a shows mixed phases of

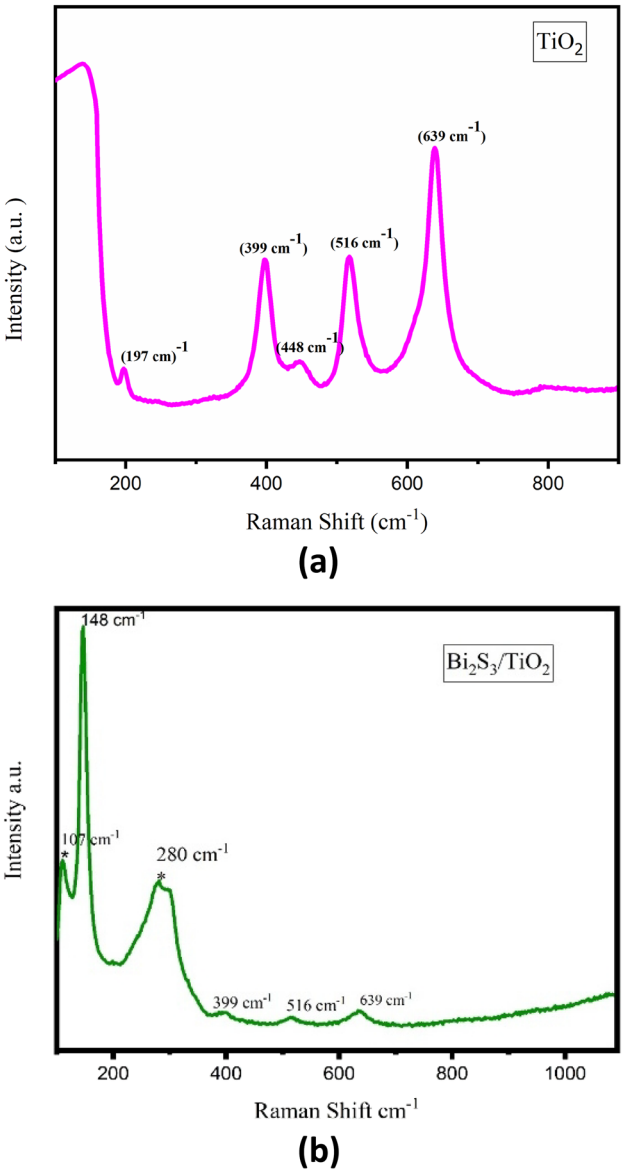

Fig. 6 **a** Raman Spectra of TiO_2 film (Deposited by doctor blade method). **b** Raman spectra of Bi_2S_3/TiO_2 photoanode

anatase and rutile TiO_2. Figure 6b) shows the Raman spectra of TiO_2/Bi_2S_3 Peaks of TiO_2 and Bi_2S_3 at 148 cm^{-1}, 399 cm^{-1}, 516 cm^{-1}, and 639 cm^{-1} confirming the formation of the anatase TiO_2 phase. The peaks at 148 cm^{-1} and 639 cm^{-1} arise mainly because of the symmetric stretching of O–Ti–O in TiO_2, the peak at 399 cm^{-1} shows the B_{1g} vibrational mode caused by symmetric bending vibration, and the peak at 516 cm^{-1} shows the A_{1g} vibrational mode, which is mainly attributed to the antisymmetric bending vibration of TiO_2 [36, 37]. The peak at 107 cm^{-1} corresponds to the

A_{1g} and 280 cm^{-1} to the B_{1g} modes, which correspond to Bi_2S_3.

3.5 JV curves

The JV curves of the Bi_2S_3/TiO_2 film using the carbon electrode (Fig. 7) shows improved photovoltaic behavior with increasing Bi_2S_3 thickness. The cell parameters of Bi_2S_3/TiO_2 films using the Carbon electrode is shown in Table 2. The open-circuit voltage (V_{oc}) increases from 0.11 to 0.14 V as the number of SILAR cycles increases from 5 to 25 cycles. The short-circuit current density (J_{sc}) peaks at 20 SILAR cycles, reaching 6.58 mA/cm^2, suggesting optimal light absorption and carrier generation. The fill factor ranged from 29.83 to 48.77%, and the highest value was achieved after 15 cycles. The overall power conversion efficiency peaked at 0.30% for 20 SILAR cycles, likely owing to non-optimal cell design and poor charge collection. Comparing the IV parameters for 15 cycles, there was a large difference in the fill factor and efficiency, possibly owing to measurement errors or variability. Overall, the IV results suggest that increasing the Bi_2S_3 thickness improves the photovoltaic behavior until the optimal point is reached after 20 SILAR cycles. Here, we varied the SILAR cycles from 5 to 25 to obtain variable performance of the solar cells. Five cycles of Bi_2S_3 on the mesoporous TiO_2 layer resulted in incomplete sensitizer coverage. As the number of deposition cycles increased, the performance of the cell increased; however, after 25 cycles, the conversion efficiency of Bi_2S_3 on TiO_2 was lower than that at 20 cycles. This may cause aggregated deposition of sensitizers. Here, we evaluate the performance of a Bi_2S_3 (20 cycles)/TiO_2 photoanode with a CTS counter electrode. Twenty deposition cycles of Bi_2S_3 on TiO_2 resulted in the optimal loading of the sensitizer (neither incomplete nor aggregated) on the TiO_2 layer. This optimized film (based on performance) was used to measure the performance of solar cells with a CTS counter electrode.

The solar cell parameters for 20 SILAR cycles of Bi_2S_3/TiO_2 were obtained using a CTS counter electrode is shown in Table 3 and JV cure as shown in Fig. 8 showing a fill factor of 0.59, an open-circuit voltage of 0.238 V, a short-circuit current density of 5.70 mA/cm^2, and a power conversion efficiency of 0.80%. The low efficiency indicates significant losses in the cell, while a fill factor of 0.59 indicates efficient charge carrier collection and low internal resistance. However, the low Jsc and efficiency suggest high recombination and low light absorption, possibly because of the insufficient thickness or poor quality of the Bi_2S_3 absorber layer. The performance parameters

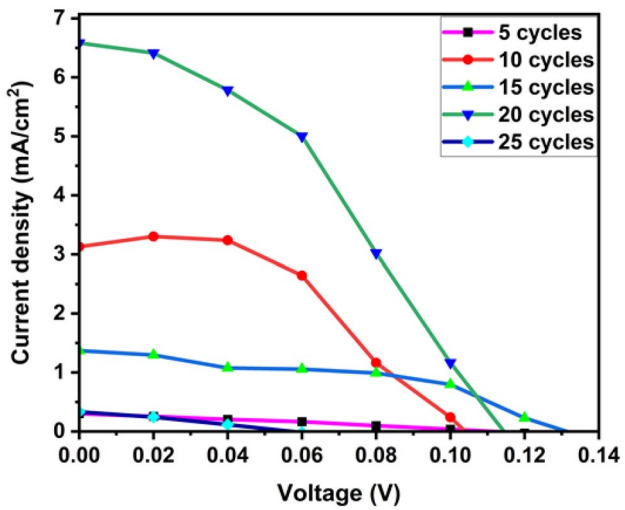

Fig. 7 Comparative JV curves of various SILAR cycles (5–20) of Bi_2S_3/TiO_2 photoanode using C counter electrode

Table 3 Solar cell parameters of Bi_2S_3/TiO_2 photoanode using CTS counter electrode

SILAR cycle	Voc (V)	Fill factor (%)	Jsc (mA/cm^2)	Efficiency (%)
20	0.23	0.59	5.70	0.80

Table 2 Solar cell parameters of Bi_2S_3/TiO_2 photoanode using C counter electrode

SILAR Cycle	I_{sc} (mA)	V_{oc} (V)	Fill Factor (%)	Jsc (mA/cm^2)	Efficiency (%)
5	0.01	0.11	29.83	0.30	0.01
10	0.05	0.13	44.20	1.37	0.07
15	0.25	0.10	48.77	3.12	0.15
20	0.13	0.11	39.83	6.58	0.30
25	0.07	0.14	34.54	2.57	0.12

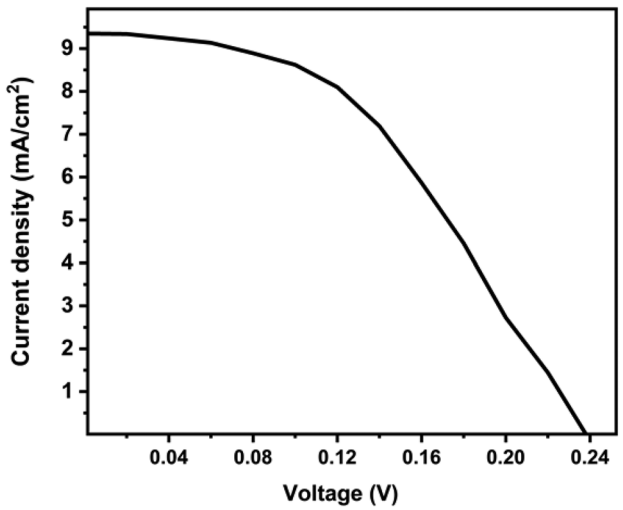

Fig. 8 JV curve of Bi_2S_3/TiO_2 with CTS counter electrode (20 SILAR cycles)

suggest that the 15 SILAR cycle Bi_2S_3/TiO_2 cell can generate a decent photovoltage, but improvements in photocurrent and power conversion are needed, likely through optimization of the Bi_2S_3 layer and interface quality.

4 Conclusion

This study reports the feasibility of using a SILAR-deposited Bi_2S_3 layer on a TiO_2 Photoanode as a sensitizer for the conversion of photons in SSSC. In this study, a Bi_2S_3/TiO_2 photoelectrode was synthesized on an FTO substrate via SILAR. SILAR-deposited Bi_2S_3 is amorphous, which is a major drawback of this method. Annealing was essential for obtaining the crystalline orthorhombic phase of Bi_2S_3. In this study, we investigated the effect of the number of SILAR cycles on the performance of Bi_2S_3/TiO_2-based solar cells. XRD analysis showed the successful deposition of orthorhombic Bi_2S_3 on tetragonal anatase/rutile TiO_2. UV–Vis absorption was extended to the visible range with Bi_2S_3 sensitization. SEM and EDS confirmed the uniform Bi_2S_3 coating on the TiO_2. The IV measurements showed increasing V_{oc}, J_{sc}, FF, and efficiency with SILAR cycles, peaking at 20 cycles. Comparing the C and CTS counters, CTS provided a higher 0.80% efficiency versus 0.30% for C. In summary, SILAR-deposited Bi_2S_3-sensitized TiO_2 to visible light absorption. Increasing the Bi_2S_3 thickness improved the performance until it reached an optimal value after 20 cycles. The CTS counter electrode provides better efficiency than C. Further improvements in the cell design are needed to increase the efficiency. The Bi_2S_3/TiO_2 heterostructure can be used for visible light-induced H_2 evolution. The eco-friendly nature and low production cost are the most promising features of Bi_2S_3/TiO_2 photoelectrodes for application in PEC hydrogen generation and photocatalysis.

Acknowledgements

Abhijit T. Supekar is thankful to the State Government of Maharashtra for financial support through the CSMNRF-2020 fellowship. Shoyebmohamad F. Shaikh extends his sincere appreciation to the Researchers Supporting Project number (RSP2024R370), King Saud University, Riyadh, Saudi Arabia, for their financial support.

Author contributions

Conceptualization: Abhijit T. Supekar (A.T.S.), Pankaj K. Bhujbal (P.K.B.), Almas M. Mujawar (A.M.M.), Sandesh R. Jadkar (S.R.J.), and Shoyebmohamad F. Shaikh (S.F.S.). Methodology: Abhijit T. Supekar (A.T.S.), Pankaj K. Bhujbal (P.K.B.), Almas M. Mujawar (A.M.M.), Sandesh R. Jadkar (S.R.J.), and Sopan. M. Rathod (S.M.R.). Writing—Original Draft Preparation: Abhijit T. Supekar (A.T.S.), Pankaj K. Bhujbal (P.K.B.), and Almas M. Mujawar (A.M.M.); Writing—Review and Editing: Sopan. M. Rathod (S.M.R.), Suhas Kowshik (S.K.), and Nithesh Naik (N.N.). Supervision: Sandesh R. Jadkar (S.R.J.) and Nithesh Naik (N.N.). All authors have read and agreed to the published version of the manuscript.

Funding

Open access funding provided by Manipal Academy of Higher Education, Manipal. Shoyebmohamad F. Shaikh extended his sincere appreciation to the Researchers Supporting Project number (RSP2024R370), King Saud University, Riyadh, Saudi Arabia, for their financial support for the project.

Data availability

The datasets generated or analyzed during the current study are available from the corresponding author upon reasonable request.

Declarations

Conflict of interest The authors declare that they have no known competing financial interests to declare.

Supplementary Information The online version contains supplementary material available at https://doi.org/10.1007/s10854-024-13181-4.

References

1. Z. Pan, H. Rao, I. Mora-Seró, J. Bisquert, X. Zhong, Quantum dot-sensitized solar cells. Chem. Soc. Rev. **47**(20), 7659 (2018). https://doi.org/10.1039/C8CS00431E
2. K.S. Shaikh, A.M. Mujawar, A.T.P.E. SupekarLokhande, J.L. Gunjakar, H.M. Pathan, Deposition of nickel doped zinc oxide/titanium oxide films and its applications towards light-harvesting device. ES Energy Environ. **22**, 992 (2023). https://doi.org/10.30919/esee992
3. K.M. Gadave, P.K. Bhujbal, D.R. Shinde, S.P. Rasale, Utilization of naturally occurring pigment lycopene as a photosensitizer for ZnO based dye-sensitized solar cells. ES Food Agrofor. **6**, 27–34 (2021). https://doi.org/10.30919/esfaf543
4. S.S. Rakhunde, K.M. Gadave, D.R. Shinde, P.K. Bhujbal, Effect of dye absorption time on the performance of a novel 2-HNDBA sensitized ZnO photo anode-based dye-sensitized solar cell. Engineered Science **12**(2), 117–124 (2020). https://doi.org/10.30919/es8d1146
5. S.D. Satpute, J.S. Jagtap, P.K. Bhujbal, S.M. Sonar, P.K. Baviskar, H.M. Pathan, Mercurochrome sensitized ZnO/In_2O_3 photoanode for dye-sensitized solar cell. ES Energy Environ. **9**(5), 89–94 (2020). https://doi.org/10.30919/esee8c720
6. S.D. Satpute, P.K. Bhujbal, S.F. Shaikh, S.A. Patil, S.R. Jadkar, S.A. More, TiO_2 blocking layer incorporated TiO_2/In_2O_3-based photoanode for DSSC application. J. Mater. Sci. Mater. Electron. **34**(36), 2311 (2023). https://doi.org/10.1007/s10854-023-11702-1
7. N.I. Beedri, P.K. Baviskar, A.T. Supekar, S.R.J. Inamuddin, H.M. Pathan, Bilayered ZnO/Nb_2O_5 photoanode for dye-sensitized solar cell. Int. J. Mod. Phys. B **32**(19), 1840046 (2018). https://doi.org/10.1142/S0217979218400465
8. W. Li, G. Jin, H.J. Li, Y. Yang, Q. Chen, Phosphotungstic acid and WO3 incorporated TiO_2 thin films as novel photoanodes in dye-sensitized solar cells. Electrochim. Acta. Acta **2015**(153), 499–507 (2015). https://doi.org/10.1016/j.electacta.2014.12.030
9. A.N. Kawade, P.K. Bhujbal, A.T. Supekar, H.M. Pathan, K.M. Sonawane, Eosin-Y sensitized tin oxide (SnO_2): fabrication and its analysis. Optik **216**, 164968 (2020). https://doi.org/10.1016/j.ijleo.2020.164968
10. A.K. Kawade, P.K. Bhujbal, A.T. Supekar, K.M. Sonawane, H.M. Pathan, S.F. Shaikh, A.A. Al-Kaitani, Comparative study of eosin-y and rose bengal sensitized SnO_2-ZnO composite electrode for dye-sensitized solar cell. ES Energy Environ. **14**, 73–78 (2021). https://doi.org/10.30919/esee8c495
11. V.P. Bhalekar, M.B. Rajendra Prasad, A.T. Supekar, Impact of number of sensitizer SILAR cycles on the performance of ZnO based PbS quantum dot-sensitized solar cells. J. Mater. Sci. Mater. Electron. **34**(31), 2083 (2023). https://doi.org/10.1007/s10854-023-11456-w
12. H. Zhang, C. Wang, W. Peng, C. Yang, X. Zhong, Quantum dot sensitized solar cells with efficiency up to 8.7% based on heavily copper-deficient copper selenide counter electrode. Nano Energy **23**, 60–69 (2016). https://doi.org/10.1016/j.nanoen.2016.03.009
13. J. Tian, T. Shen, X. Liu, C. Fei, L. Lv, G. Cao, Enhanced performance of PbS-quantum dot-sensitized solar cells via optimizing precursor solution and electrolytes. Sci. Rep. **6**(1), 23094 (2016). https://doi.org/10.1038/srep23094

14. G. Mnasri, S. Mansouri, M. Yalçin, L. El Mir, A.A. Al-Ghamdi, F. Yakuphanoglu, Characterization and study of CdS quantum dots solar cells based on graphene-TiO_2 nanocomposite photoanode. Results Phys. **18**, 103253 (2020). https://doi.org/10.1016/j.rinp.2020.103253
15. Y. Ma, H. Li, J. Yuan, In-situ solution chemical reaction deposition of Bi_2S_3 quantum dots on mesoscopic TiO2 films for application in quantum-dot-sensitized solar cells. Integr. Ferroelectr.. Ferroelectr. **169**, 42–49 (2016). https://doi.org/10.1080/10584587.2016.1162610
16. S.S. Pramana, E.L. Gui, A.M. Kang, N. Yantara, N. Mathews, S. Mhaisalkar, Effect of TiO_2 mesoporous layer and surface treatments in determining efficiencies in antimony sulfide-(Sb_2S_3) sensitized solar cells. J. Electrochem. Soc.Electrochem. Soc. **159**, B247–B250 (2012). https://doi.org/10.1149/2.007203jes
17. N.S. Yesugade, C.D. Lokhande, C.H. Bhosale, Structural and optical properties of electrodeposited Bi_2S_3, Sb_2S_3 and As_2S_3 thin films. Thin Solid Films **263**(2), 145–149 (1995). https://doi.org/10.1016/0040-6090(95)06577-6
18. C.D. Lokhande, A.U. Ubale, P.S. Patil, Thickness-dependent properties of chemically deposited Bi_2S_3 thin films. Thin Solid Films **302**(1–2), 1–4 (1997). https://doi.org/10.1016/S0040-6090(96)09540-5
19. A.T. Supekar, P.K. Bhujbal, S.A. Salunke, S.M. Rathod, S.P. Patole, H.M. Pathan, Bismuth sulfide and antimony sulfide-based solar cells: a review. ES Energy Environ. **19**, 848 (2023). https://doi.org/10.30919/esee8c848
20. A.A. AL-Zahrani, Z. Zainal, Z.A. Talib, H.N. Lim, L. MohdFudzi, A.M. Holi, Synthesis of binary Bi_2S_3/ZnO nanorod array heterostructure and their photoelectrochemical performance. J. Nanomater.Nanomater. **1**, 5212938 (2019). https://doi.org/10.1155/2019/5212938
21. Y. Wang, J. Chen, L. Jiang, F. Liu, Y. Lai, J. Li, Characterization of Bi2S3 thin films synthesized by an improved successive ionic layer adsorption and reaction (SILAR) method. Mater. Lett.Lett. **209**, 479–482 (2017). https://doi.org/10.1016/j.matlet.2017.08.039
22. V.V. Killedar, C.D. Lokhande, C.H. Bhosale, Preparation and characterization of Bi_2S_3 thin films spray deposited from non-aqueous media. Thin Solid Films **289**(1–2), 14–16 (1996). https://doi.org/10.1016/S0040-6090(96)08868-2
23. W.M. Linhart, S.J. Zelewski, P. Scharoch, F. Dybała, R. Kudrawiec, Nesting-like band gap in bismuth sulfide Bi_2S_3. J. Mater. Chem. C **9**(39), 13733–13738 (2021). https://doi.org/10.1039/D1TC03625D
24. I. Hwang, K. Yong, Counter electrodes for quantum-dot-sensitized solar cells. Chem. Electro. Chem. **2**(5), 634653 (2015). https://doi.org/10.1002/celc.201402405
25. L.H. Kharboot, N.A. Fadil, T.A.A. Bakar, A.S.M. Najib, N.H. Nordin, H. Ghazali, A review of transition metal sulfides as counter electrodes for dye-sensitized and quantum dot-sensitized solar cells. A Mater. **16**(7), 2881 (2003). https://doi.org/10.3390/ma16072881
26. B. Zhao, S. Li, M. Che, L. Zhu, Synthesis of Cu_3SnS_4 nanoparticles with a novel structure as low-cost counter electrode in dye-sensitized solar cell Int. J. Electrochem. Sci. **11**(8), 2881 (2016). https://doi.org/10.20964/2016.08.29
27. M.B. Rajendra Prasad, H.M. Pathan, Room temperature synthesis of rutile titania nanoparticles: a thermodynamic perspective. Eur. Phys. J. D **2014**(68), 1–5 (2014). https://doi.org/10.1140/epjd/e2013-40268-1
28. H.D. Shelke, A.C. Lokhande, V.S. Raut, A.M. Patil, J.H. Kim, C.D. Lokhande, Facile synthesis of Cu2SnS3 thin films grown by SILAR method: effect of film thickness. J. Mater. Sci. Mater. Electron. **28**, 7912–7921 (2017). https://doi.org/10.1007/s10854-017-6492-7
29. H.D. Shelke, A.C. Lokhande, A.M. Patil, J.H. Kim, C.D. Lokhande, Cu_2SnS_3 thin film: structural, morphological, optical and photoelectrochemical studies. Surfaces and Interfaces. **9**, 238–244 (2017). https://doi.org/10.1016/j.surfin.2017.08.006
30. M.R. Prasad, P.S. Tamboli, R.V. Ingle, K.D. Diwate, P.K. Baviskar, B.R. Sankpal, K.C. Mohite, S.R. Jadkar, H.M. Pathan, Geometrical thickness of titania photoanode as an influential parameter in controlling the photovoltaic performance of CdS quantum dot sensitized solar cells. Curr. Appl. Phys.. Appl. Phys. **17**(12), 1691–1698 (2017). https://doi.org/10.1016/j.cap.2017.09.009
31. S.M. Sonar, P.K. Baviskar, H.M. Pathan, P.B. Ahirrao, Chemically synthesized Bi_2S_3, CuS, and Bi_2S_3/CuS heterostructure materials as counter electrode: Dye-sensitized solar cell application. Ind. J. Pure Appl. Phys. **59**(2), 143–149 (2021). https://doi.org/10.56042/ijpap.v59i2.40445
32. P.R. Nikam, P.K. Baviskar, J.V. Sali, K.V. Gurav, J.H. Kim, B.R. Sankapal, SILAR coated Bi_2S_3 nanoparticles on vertically aligned ZnO nanorods: synthesis and characterizations. Ceram. Int.nt. **41**(9), 10394–10399 (2015). https://doi.org/10.1016/j.ceramint.2015.03.239
33. H. McDaniel, N. Fuke, N.S. Makarov, J.M. Pietryga, V.I. Klimov, An integrated approach to realizing high-performance liquid-junction quantum dot sensitized solar cells. Nat. Commun.Commun. **4**(1), 2887 (2013). https://doi.org/10.1038/ncomms3887
34. S. Li, J. Huang, X. Ning, Y. Chen, Q. Shi, TiO_2/Bi_2S_3 ball-and-stick structure heterojunction prepared on FTO glass as a photoanode for solar cells. J. Iran. Chem. Soc. **16**, 231–241 (2019). https://doi.org/10.1007/s13738-018-1501-1

35. G. Huang, J. Zhang, F. Jiang, Z. Zhang, J. Zeng, X. Qi, Z. Shen, H. Wang, Z. Kong, J. Xi, Z. Ji, Excellent photoelectrochemical activity of Bi2S3 nanorod/TiO2 nanoplate composites with dominant 001 facets. J. Solid State Chem. **281**, 121041 (2020). https://doi.org/10.1016/j.jssc.2019.121041
36. S. Paul, S. Ghosh, D. Barman, S.K. De, Maximization of photocatalytic activity of Bi2S3/TiO2/Au ternary heterostructures by proper epitaxy formation and plasmonic sensitization. Appl. Catal. BCatal. B **219**, 287–300 (2017). https://doi.org/10.1016/j.apcatb.2017.07.057
37. U.G.E.N. Balachandran, N.G. Eror, Raman spectra of titanium dioxide. J. Solid State Chem. **42**(3), 276–282 (1982). https://doi.org/10.1016/0022-4596(82)90006-8